A projection based method for shape measurement

Thanh Phuong Nguyen, Xuan Son Nguyen, Mohamed Anouar Borgi, M K Nguyen

Noname manuscript No.
(will be inserted by the editor)

A projection based method for shape measurement

Thanh Phuong Nguyen · Xuan Son Nguyen · Mohamed Anouar Borgi · M. K. Nguyen

the date of receipt and acceptance should be inserted later

Abstract This work addresses two main contributions for shape measurement. First, a new circularity measure for planar shapes is introduced based on their geometrical properties in the projection space of Radon transform. Second, a general-purpose evaluation criterion, Power Of Discrimination (POD), for assessing the efficiency of a shape measure is proposed. The new measure ranges over the interval [0,1], and produces the value 1 if and only if the measured shape is a perfect circle. The proposed measure is invariant with respect to translation, rotation and scaling transformations. Moreover, it is also robust against border distortion of shapes. It is theoretically well founded and can be extended to other problems of shape measurement. Our approach can deal with complex shapes composed of connected components that cannot be handled by classical contour-based methods. Several experiments show its good behavior and demonstrate the efficiency and applicability of our proposed measure. Finally, we also consider our proposed evaluation criterion for assessing different circularity measures.

Keywords circularity · shape measurement · evaluation criterion

1 Introduction

Object recognition is an important area of computer vision. Object comparison is often carried out by mapping objects of interest onto feature spaces to reduce the calculation complexity and to enhance the discriminant power.

Corresponding author: Thanh Phuong Nguyen, E-mail: nguyenthanhphuong1@tdtu.edu.vn; Thanh Phuong Nguyen is with AI Lab, Faculty of Information Technology, Ton Duc Thang University, Ho Chi Minh City, Vietnam; Université de Toulon, Aix Marseille Université, CNRS, LIS, Marseille, France. · X.S. Nguyen is with Université de Caen Normandie, CNRS, GREYC, UMR 6072, 14032 Caen, France · Mohamed Anouar Borgi is with Research Groups on Intelligent Machines, University of Sfax, BP 1173, Sfax 3038, Tunisia · M. K. Nguyen is with ETIS, ENSEA/Université de Cergy-Pontoise/CNRS UMR 8051, 95302 Cergy-Pontoise, France.

This process generally relies on object's appearance properties. Among different appearance properties, shape is widely utilized for object description and classification thanks to its high discriminant power. However, conception of a good shape descriptor remains a difficult problem even though numerous of methods have been introduced to address this problem. According to Rosin [1], there are three main challenges in defining a shape descriptor: 1) the robustness of the descriptor against variations among shapes of the same class; 2) the insensitivity of the descriptor to similarity transformations such as translation, rotation, and scaling; 3) the invariance of the descriptor to other transformations such as affine transformation on triangles or aspect ratio adjustment on rectangles.

Generally, there are two main approaches to design shape descriptors: general purpose shape descriptors and specific shape estimators. The first one is based on different transforms such as Fourier transform [2], Hough transform [3], Radon transform [4], dominant points [5], similarity map [6], graph-based representation [7], and image moments [8] to describe shapes. More different methods have been addressed in this survey [9]. This approach producing high-dimensional feature vectors is suitable for generic applications such as shape retrieval [10,11,12], shape and curve matching [13,14,15]. The second one measures or estimates geometrical properties of shapes and thus the descriptors in this approach often have clear geometric interpretations such as measurements of ellipticity [16,17,1], circularity [18,19,20,21,22,23,24,25,26, 27,28,29,30] , polygonality [31], triangularity [1], rectangularity [1,32], linearity [32], orientability [33,34].

We address in this paper two main following contributions. First, a novel approach for circularity measurement of a shape is introduced. Second, we propose a general-purpose evaluation criterion for assessing shape measures. Our approach exploits some beneficial geometric properties of circles in the projection space. In the literature, the projection-based approach has been used for different problems of shape measurement such as polygonality [31], geometrical feature extraction [35], extraction of geometrical properties and spatial relations [36], triangularity measurement [1], orientation [37], convex-set perimeter estimation [38] and reflectional symmetry detection [39]. It should be remarked that we exploit the projection data in a totally different way compared to these works. The main idea is to introduce an invariant property of a perfect circle and then to estimate how far it is degraded for a given shape. The obtained measures take value in $[0, 1]$ and are robust to additive noise, boundary distortion, and similarity transformation. Using this projection-based approach, our method can deal with complex shapes composed of several closed contours or shapes having very noisy boundaries. Because the classical methods using contour-based approach consider a shape as a closed contour, they cannot be used for these cases.

The rest of this paper is organized as follows. Section 2 reviews some recents advances in shape measurement and also in evaluation of shape measures. Section 3 firstly recalls Radon transform, its properties and introduces several useful notations in Sections 3.1, 3.1.2, and then develops a theoreti-

cal foundation for the proposed approach in Section 3.2 that is the base for our circularity measure presented in Section 4. Section 5 introduces a novel evaluation criterion for assessing shape measures. The next section shows experimental results of the proposed methods. Several conclusions are given in the last section.

2 Related work

2.1 Shape measures

The measurement approach, which often deals with a single characteristic of shapes, estimates geometrical properties of shapes. It can be classified in two main groups. The first one estimates the similarity between a shape and a geometrically pre-defined shape to obtain a similarity measure such as circularity, ellipticity, polygonality [31], rectangularity or triangularity [1]. Ellipticity measurement has been considered in [1,16,17] using different methods such as Fourier transform [16], elliptic variance [17], moment invariants [1]. Rectangularity, which measures the similarity between a shape and a rectangle, has been studied using minimum-area encasing rectangle (MAER) of a shape [1] or rectangular templates [32]. The second one measures some geometrical properties of shape such as orientation, symmetry or linearity. Measuring shape's orientation has been considered in many works using curvature weighted gradient [33], boundary information [34] or dominant orientation [40]. Symmetry detection that determines whether a shape possesses reflectional and rotational symmetries is also an important topic in shape analysis. Different methods have been introduced using Fourier transform [41], phase congruency calculated from Gabor wavelets [42] or image moments [43]. Linearity, which measures the similarity between an open curve and a straight segment, has also been studied in different works [44,45].

Among different shape measurement methods, measuring circularity or compactness of a shape is a prominent approach because circle is a basic shape that appears in a vast range of image processing tasks. The methods in this research direction response to the problem: How much a given shape differs from a perfect circle. Several methods [18,19,20,21,22,23,24,25,26,27,28,29,30] have been proposed in the literature to deal with this problem. The classic measure based on non-compactness measure [18] using perimeter and area of the shape ($4\pi A/P^2$) is not satisfactory in reality because it is not really scale invariant and it can reach the perfect value for non circular shapes. Most of the works define circularity based on different geometric properties of circles. In general, there are two main following approaches for circularity measurement: contour-based and region-based approaches. The first direction contains the methods exploiting desirable properties of circular shapes [19, 22,27,28,29] by taking into account their boundary properties: distances from centroid to boundary [19], Fourier transform (DFT) on boundary contour [22], separating circle problem [27,28], polygon similarity [29], linearity of boundary

points in polar coordinate system [25], integer interval from boundary representation [46], etc. These methods can only deal with simple shapes and are generally sensible against non-linear deformations. The second one consists of methods [20,21,23,24,47] that define circularity measurement by studying the region of shape. Different geometric properties have been addressed to characterize the region of a disk such as distance map [20,21], moment [47,24,48] or area [49]. In this direction, moment is popular feature to describe region of shape due to its robustness to noise and deformation. Different moments have been taken into account: affine moment invariance [23], invariant Hu moment [24], 3D polar-radius-moment invariance [47], or Kullback-Leibler divergence of uniform probability density on shape region [48]. The methods in the second direction have generally their performance superiority in the case of shape boundary defects compared to those of the first one.

2.2 Evaluation of shape measures

There is not many works related to this topic in the literature. For assessing rectangularity measures, Rosin [50] applied them to some parametrized synthetic shapes to track the rectangularity values when the shapes are continuously modified. A similar idea was used in [1] for evaluating triangularity and ellipticity. In [51], the classification rate of the descriptor based on a shape measure on a dataset was used for assessing this measure. However, to the best of our knowledge, there is not an evaluation criterion for comparing different shape measures like assessing of polygonalization methods. Sarkar [52] introduced Figure of Merit (FOM) to balance between the error approximation and the compression ratio. Rosin [53] proposed Merit criterion by comparing with optimal results.

3 Projection-based circularity measurement

3.1 Radon transform for shape representation

We recall in this section the Radon transform and then present a common way to use this transform as an effective tool for shape representation which has been exploited in different works [4,54] on shape analysis.

3.1.1 Radon transform

Let $f(x,y) \in \mathbb{R}^2$ be a 2D function and $L(\theta,\rho)$ be a straight line in $\mathbb{R}^2$ represented by

$$L = \{(x,y) \in \mathbb{R}^2 : x\cos\theta + y\sin\theta = \rho\} \tag{1}$$

where θ is the angle L makes with the y axis and ρ is the distance from the origin to L. The Radon transform [55] of f, denoted by $\mathcal{R}_f$, is a function

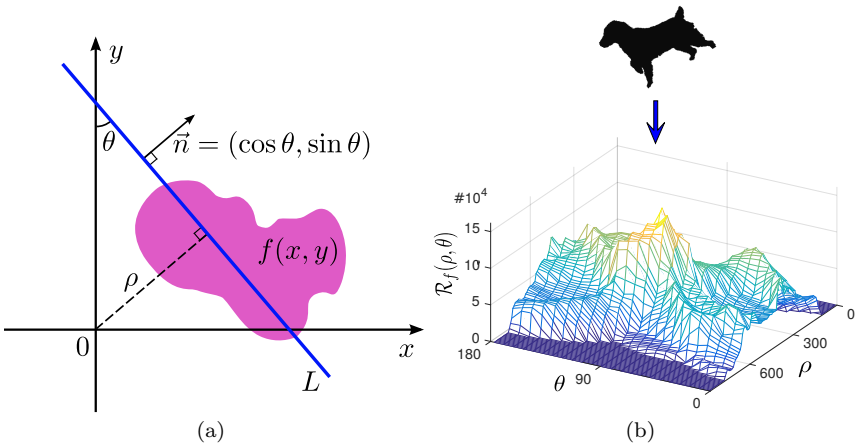

(a) (b)

Fig. 1: : (a)- Graphical illustration of the Radon transform of a function $f(x, y)$; (b)- A dog shape $\mathcal{D}$ and its representation in the projection space.

defined on the space of lines $L(\theta, \rho)$ by the line integral along each line:

$$\mathcal{R}_f(\theta,\rho) = \int_{L(\theta,\rho)} f(x,y)\,\mathrm{d}x\mathrm{d}y = \int_{-\infty}^{\infty}\int_{-\infty}^{\infty} f(x,y)\,\delta(\rho - x\cos\theta - y\sin\theta)\,\mathrm{d}x\mathrm{d}y. \quad (2)$$

In the field of shape analysis and recognition, the function $f(x, y)$ is constrained to the following particular definition:

$$f(x,y) = \begin{cases} 1 & \text{if } x \in \mathcal{D} \\ 0 & \text{otherwise,} \end{cases} \quad (3)$$

where $\mathcal{D}$ is the domain of the binary shape represented by $f(x, y)$. In the illustration of the Radon transform in Figure 1.a, the shaded region represents the region $\mathcal{D}$. The value of the line integral in Equation (2) is equal to the length of the intersection between the line L and the shaded region. Figure 1.b shows also the Radon transform $\mathcal{R}_f(\theta, \rho)$ on a binary domain of a dog shape.

3.1.2 Notations and significances

For each projection direction θ, the radial distances ρ_1^θ and ρ_2^θ are respectively defined as $\rho_1^\theta = \inf\{\rho \mid \mathcal{R}_\mathcal{D}(\theta,\rho) > 0\}$ and $\rho_2^\theta = \sup\{\rho \mid \mathcal{R}_\mathcal{D}(\theta,\rho) > 0\}$. The "profile" of $\mathcal{D}$ in the direction θ, denoted as $C_\mathcal{D}^\theta$, is defined as $\mathcal{R}_\mathcal{D}(\theta, \rho_1^\theta{:}\rho_2^\theta)$. More precisely, $C_\mathcal{D}^\theta(\rho - \rho_1^\theta) = \mathcal{R}_\mathcal{D}(\theta,\rho)$, $\forall\rho \in [\rho_1^\theta, \rho_2^\theta]$ (see Figure 2). The "axis distance" of $\mathcal{D}$ in the direction θ, denoted as ρ_0^θ, is defined as $\rho_0^\theta(\mathcal{D}) =$

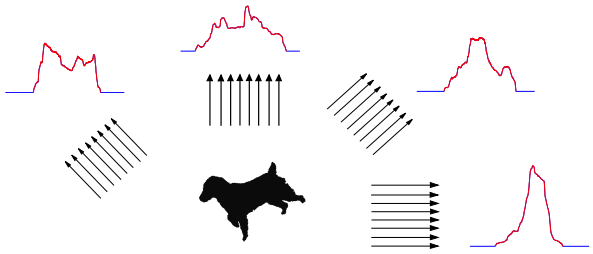

Fig. 2: A dog shape $\mathcal{D}$ and its projections in different directions: 0, $\frac{\pi}{4}$, $\frac{\pi}{2}$, $\frac{3\pi}{4}$. The corresponding profiles, $C^0_{\mathcal{D}}$, $C^{\frac{\pi}{4}}_{\mathcal{D}}$, $C^{\frac{\pi}{2}}_{\mathcal{D}}$ and $C^{\frac{3\pi}{4}}_{\mathcal{D}}$ are in red.

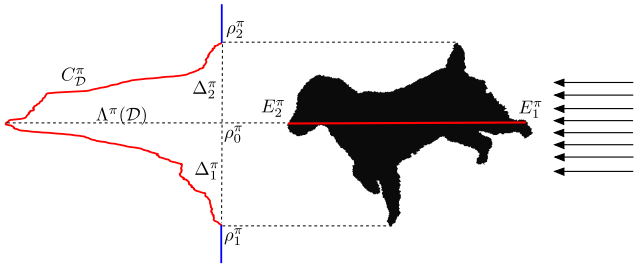

Fig. 3: A dog shape $\mathcal{D}$ and its related notations (ρ_0^θ, ρ_1^θ, ρ_2^θ, $\Lambda^\theta(\mathcal{D})$, $\Delta_1^\theta(\mathcal{D})$, $\Delta_2^\theta(\mathcal{D})$, $E_1^\theta(\mathcal{D})$, $E_2^\theta(\mathcal{D})$) in direction π. $C^\theta(\mathcal{D})$ and the integral line corresponding to $\Lambda^\theta(\mathcal{D})$ are in red.

$\underset{\rho}{\text{argmax}}\ \mathcal{R}_{\mathcal{D}}(\theta,\rho)$, $\forall\rho \in [\rho_1^\theta, \rho_2^\theta]$. The two extremities in the boundary of $\mathcal{D}$ corresponding to $\rho_0^\theta(\mathcal{D})$ are denoted as E_1^θ and E_2^θ, respectively. In addition, the "length" of $\mathcal{D}$ in the direction θ, denoted as $\Lambda^\theta(\mathcal{D})$, is defined as $\Lambda^\theta(\mathcal{D}) = \mathcal{R}_{\mathcal{D}}(\theta, \rho_0^\theta)$. The left and right "projected bands" of $\mathcal{D}$ in the direction θ, denoted as $\Delta_1^\theta(\mathcal{D})$ and $\Delta_2^\theta(\mathcal{D})$, are then determined as $\Delta_1^\theta(\mathcal{D}) = |\rho_0^\theta - \rho_1^\theta|$ and $\Delta_2^\theta(\mathcal{D}) = |\rho_2^\theta - \rho_0^\theta|$. For the simplicity of presentation, from now on, we denote $\mathcal{R}_f(\theta,\rho)$ by $\mathcal{R}_{\mathcal{D}}(\theta,\rho)$, where function f is defined on domain $\mathcal{D}$ by Equation (3). Figure 3 illustrates the above notations considering a dog shape in direction π.

These notations allow to deal with a column θ of $\mathcal{D}$'s Radon image. First, $C^\theta_{\mathcal{D}}$ indicates the non-zero part of this column. Second, $\Lambda^\theta(\mathcal{D})$ and ρ_0^θ indicate the maximal value and its position while Δ_1^θ and Δ_2^θ determine the non-zero bands corresponding to a decomposition of $C^\theta_{\mathcal{D}}$ at ρ_0^θ.

3.2 Representation of a circle and its invariant properties in Radon space

Using the notations and definitions in Section 3.1, this section presents some theoretical results on the appearance of circular shapes in Radon space. These

results can be used to distinguish circles from non-circular shapes and are the basis for the proposal of circularity measure in Section 4.

Let us consider the Radon transform $\mathcal{R}_f(\theta,\rho) = \mathcal{R}_\zeta(\theta,\rho)$, where ζ is a circle of radius r. Without loss of generality, we suppose that ζ is centered at the origin of coordinate system. We then introduce the following properties of ζ.

Property 1 $\mathcal{R}_\zeta(\theta,\rho) = 2\sqrt{r^2-\rho^2}$.

Proof The transform is given by the length of a chord at a distance ρ from the center and it is independent of the angle θ. In addition, it is well-known that the chord length of ζ at a distance ρ from the center is $2\sqrt{r^2-\rho^2}$.

We have then the following invariant properties of ζ.

Property 2 $\Lambda^\theta(\zeta) = 2r$

Proof Because ζ is centered at the origin of coordinate system and ζ is symmetric for every direction θ, it is evident that $\rho_0 = 0$. Thanks to Property 1, $\Lambda^\theta(\zeta) = \mathcal{R}_f(\theta,\rho) = 2\sqrt{r^2-\rho_0^2}$. Because of $\rho_0 = 0$, we have $\Lambda^\theta(\zeta) = 2r$.

We remark that only the result of Property 2 is not sufficient by considering Remark 1.

Remark 1 An arbitrary shape $\mathcal{D}$ satisfying the following condition $\frac{1}{2}\Lambda^\theta(\mathcal{D}) = r, \forall\theta \in [0,\pi)$ is not necessarily a circle.

Proof Let us consider a counter-example with a Reuleaux triangle, formed from the intersection of three circular disks of radius r, where each circle has its center on the boundary of the other two (see Figure 17). It is evident that the separation of every two parallel supporting lines is r, independent of their orientation.

An another counter-example is an annulus that also satisfies Propperty 2.

In order to address the necessary conditions for a shape to become a circle, we present hereafter following propositions defining geometric properties of circular shapes and also necessary conditions of an arbitrary shape in projection space to become a circular disk.

Proposition 1 $\Delta_1^\theta(\zeta) = \Delta_2^\theta(\zeta) = r$

Proof It is evident that $\rho_1^\theta = -r$ and $\rho_2^\theta = r, \forall\theta \in [0,2\pi)$ because ζ is a centered circle at the origin of coordinate system. Therefore, $\Delta_1^\theta = \Delta_2^\theta = r$ due to $\rho_0^\theta = 0$.

So, $\Lambda^\theta(\zeta)$, Δ_1^θ and Δ_2^θ are invariant with respect to θ.

We consider now the necessary conditions for an arbitrary shape $\mathcal{D}$ to become a circle. Let us consider an arbitrary shape $\mathcal{D}$ satisfying the following condition $\frac{1}{2}\Lambda^\theta(\mathcal{D}) = \Delta_1^\theta(\mathcal{D}) = \Delta_2^\theta(\mathcal{D}) = r, \forall\theta \in [0,\pi)$. In the following, we will show that this condition is sufficient for $\mathcal{D}$ to become a circular disk. This inverse problem is addressed hereafter in Proposition 2. Please also refer to necessary materials (Lemmas 1, 2, 3, 4) in Appendix section A for more details in its proof.

Proposition 2 *An arbitrary shape $\mathcal{D}$ satisfying the following condition $\frac{1}{2}\Lambda^\theta(\mathcal{D}) = \Delta_1^\theta(\mathcal{D}) = \Delta_2^\theta(\mathcal{D}) = r, \forall\theta \in [0,\pi)$ is a circle of radius r.*

Proof Suppose that O (resp. O^θ) is the intersection between $E_1^0E_2^0$ and $E_1^{\frac{\pi}{2}}E_2^{\frac{\pi}{2}}$ (resp. $E_1^\theta E_2^\theta$ and $E_1^{\theta+\frac{\pi}{2}}E_2^{\theta+\frac{\pi}{2}}$) (please see Section 3.1.2 for the definitions of E_1^θ and E_2^θ). Let us show that $OO^\theta = 0, \forall\theta \in [0,\pi)$.

There are two following possible cases. First, $\mathcal{D}$ is a convex shape. It could be deduced from Lemma 2 that $O^\theta \equiv O^{\theta+\frac{\pi}{2}}$, and moreover due to the symmetry (the arguments applied for direction $\theta, \theta < \frac{\pi}{2}$ can be also used for direction $\frac{\pi}{2} - \theta$), it is sufficient to show $OO^\theta = 0, \forall\theta \in [0, \frac{\pi}{4})$. We consider now a sequence, defined as follows: $\{\theta\}_{i=0}^n, \theta_i = i * \frac{\pi}{4n}, \forall 0 \leq i \leq n$. Suppose that $k = \lfloor\frac{\theta}{\frac{\pi}{4n}}\rfloor$, $k < n$. Thanks to Lemma 3, we have $|O^{\theta_i}O^{\theta_{i+1}}| < \sqrt{2}r(\sqrt{5-4\cos(\frac{\pi}{4n})}-1)$ and $|O^{\theta_k}O^\theta| < \sqrt{2}r(\sqrt{5-4\cos(\frac{\pi}{4n})}-1)$. Therefore, $|OO^\theta| \leq \sum_{i=0}^{k-1}|O^{\theta_i}O^{\theta_{i+1}}| + |O^{\theta_k}O^\theta| < n\sqrt{2}r(\sqrt{5-4\cos(\frac{\pi}{4n})}-1)$. Thanks to Lemma 4, we deduce that $\lim_{n\to+\infty}|OO^\theta| = 0$. Because $|OO^\theta|$ is independent of n, so we have the following conclusion $|OO^\theta| = 0$. This result means that $\mathcal{D}$ is a circle.

In the second case, $\mathcal{D}$ is not a convex shape. Therefore, this shape must contain some concave parts and/or it contains some holes. Figure 4 illustrates shape $\mathcal{D}$ consisting of a hole in its interior. Thanks to Lemma 1, its convex hull $\mathcal{D}_1 = CV(\mathcal{D})$ satisfies the same condition as $\mathcal{D}$: $\frac{1}{2}\Lambda^\theta(\mathcal{D}_1) = \Delta_1^\theta(\mathcal{D}_1) = \Delta_2^\theta(\mathcal{D}_1) = r, \forall\theta \in [0,\pi)$. By applying the same argument as in the first case, we deduce that $\mathcal{D}_1$ is a circle of radius r. Indeed, because the convex hull of $\mathcal{D}$ (*i.e.* $\mathcal{D}_1$) is a circle, we can deduce that a possible concave part of $\mathcal{D}$ can be considered as a hole inside of $\mathcal{D}_1$ that touches its border at only one point (if not, $\mathcal{D}_1$ cannot be a circle). Now, considering the direction t passing a hole and the center of $\mathcal{D}_1$ (see Figure 4). Because $\mathcal{D}_1$ is a circle, it is evident that in the direction t, all projected value is smaller than the diameter of this circle. It means that, $\frac{1}{2}\Lambda^t(\zeta) < r$. This contradiction implies that the second case is not possible and therefore the proposition is proved.

4 Circularity measuring

The theoretical foundation, developped in Section 3, allows us to determine how a shape $\mathcal{D}$ is similar to a circle. Based on Propositions 1, 2, we will estimate the circularity measure for $\mathcal{D}$ by relying on the assumption that the more $\mathcal{D}$ is similar to a circle, the more its profiles $\frac{1}{2}\Lambda^\theta(\mathcal{D})$, $\Delta_1^\theta(\mathcal{D})$, $\Delta_2^\theta(\mathcal{D})$ *take a constant value* r. The circularity measure will be defined based on the deviation of these profiles. It should be noted that thanks to the first two properties of Radon transform (see Section 3.1), we only need to perform the projection at $\theta \in [0,\pi)$.

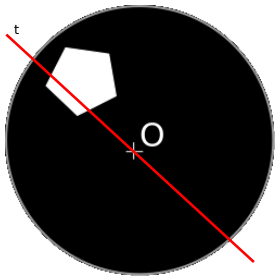

Fig. 4: $\mathcal{D}$ is not a convex shape.

4.1 Circularity measure

Let p be a profile, $\mu(p)$ and $\sigma(p)$ be respectively the mean value and standard deviation of p. Based on Propositions 1, 2, a new definition of circularity measure is introduced in Definition 1 by determining the deviation of the union of three profiles $\frac{1}{2}\Lambda^\theta(\mathcal{D})$, $\Delta_1^\theta(\mathcal{D})$, $\Delta_2^\theta(\mathcal{D})$, noted as $U_\Theta^1(\mathcal{D})$. The value r can be simply estimated as the mean value of this profile. By determining the deviation of the profile $U_\theta(\mathcal{D})$, we can measure how far $\mathcal{D}$ is similar to a circle. Moreover, with a same deviation, the more r is greater, the more $\mathcal{D}$ is closer to a real circle. Our circularity measure is then proposed as follows.

Definition 1 Let us denote $U_\Theta^1(\mathcal{D}) = \{\frac{1}{2}\Lambda^\theta(\mathcal{D}), \Delta_1^\theta(\mathcal{D}), \Delta_2^\theta(\mathcal{D})\}_{\theta\in\Theta}$. The circularity measure of $\mathcal{D}$ is defined as

$$CM(\mathcal{D}) = e^{-\frac{\sigma(U_\Theta^1(\mathcal{D}))}{\mu(U_\Theta^1(\mathcal{D}))}} \tag{4}$$

$CM(\mathcal{D})$ measures how far $\mathcal{D}$ differs from a perfect circle. The greater the ratio $\frac{\sigma}{\mu}$ is, the more $CM(\mathcal{D})$ reaches to 0 and the more $\mathcal{D}$ is linear. By definition of $CM(\mathcal{D})$, it is evident that the proposed circularity measure ranges over the interval [0,1]. It takes 1 if $\mathcal{D}$ is a perfect circle; it takes 0 if $\mathcal{D}$ is empirically considered as a linear shape.

Algorithm 1 is then introduced to measure the circularity of a shape $\mathcal{D}$ using Definition 1. Theoretically, Algorithm 1 works well and estimates the circularity of a shape. In practice, however, the calculation of $\Lambda^\theta(\mathcal{D})$, $\Delta_1^\theta(\mathcal{D})$, $\Delta_2^\theta(\mathcal{D})$ by determining the maxima of $C_\mathcal{D}^\theta$ profile can have several issues. First, the maxima may not be unique. Second, due to the boundary distortion of $\mathcal{D}$, the maxima of $C_\mathcal{D}^\theta$ may be obtained at a location that is far away the midpoint of $C_\mathcal{D}^\theta$ and then it makes a considerable disparity between $\Delta_1^\theta(\mathcal{D})$ and $\Delta_2^\theta(\mathcal{D})$.

We conduct the following simple idea to make the circularity measurement more robust against numerical issues, raised by Definition 1. Instead of estimating $\Delta_1^\theta(\mathcal{D})$, $\Delta_2^\theta(\mathcal{D})$ which are the origin of those issues, we detect the borders ρ_1^θ and ρ_2^θ of the "projected band" in direction θ. It should be noted that $\rho_2^\theta - \rho_1^\theta = \Delta_1^\theta(\mathcal{D}) + \Delta_2^\theta(\mathcal{D})$. Therefore, the problem is to verify the devia-

Algorithm 1 Circularity measurement of a shape $\mathcal{D}$.

Input: $\mathcal{D}$ – arbitrary shape, n – number of projection directions
Output: $CM(\mathcal{D})$ – circularity measure

1: $\Theta = \{\theta_i\}_{i=0}^{n-1}$, $\theta_i = i\frac{\pi}{n}$
2: Determine $\mathcal{R}(\mathcal{D})$ -Radon image of $\mathcal{D}$
3: **for** $\theta_i \in \Theta$ **do**
4: From $\mathcal{R}(\mathcal{D})$, determine $\frac{1}{2}\Lambda^{\theta_i}(\mathcal{D})$, $\Delta_1^{\theta_i}(\mathcal{D})$, $\Delta_2^{\theta_i}(\mathcal{D})$
5: **end for**
6: $U_\Theta^1(\mathcal{D}) = \{u_i\}_{i=0}^{3n-1}$, where $u_j = \frac{1}{2}\Lambda^{\theta_j}(\mathcal{D})$, $u_{j+n} = \Delta_1^{\theta_j}(\mathcal{D})$, $u_{j+2n} = \Delta_2^{\theta_j}(\mathcal{D})$, $\forall 0 \leq j < n$
7: $\sigma(\mathcal{D}) = \frac{1}{3n}\sum_{i=0}^{3n-1} u_i$
8: $\mu(\mathcal{D}) = \sqrt{\frac{1}{3n}\sum_{i=0}^{3n-1}(u_i - \sigma(\mathcal{D}))^2}$
9: $CM(\mathcal{D}) = e^{-\frac{\sigma(\mathcal{D})}{\mu(\mathcal{D})}}$

tion of the profiles $\rho_2^\theta - \rho_1^\theta$, $\Lambda^\theta(\mathcal{D})$ and $\mathcal{R}_\mathcal{D}(\theta, \frac{\rho_1^\theta + \rho_2^\theta}{2})$. It is theoretically verified by the following proposition.

Proposition 3 *An arbitrary shape $\mathcal{D}$ satisfying the following condition $\frac{1}{2}\Lambda^\theta(\mathcal{D}) = \frac{1}{2}\mathcal{R}_\mathcal{D}(\theta, \frac{\rho_1^\theta+\rho_2^\theta}{2}) = \frac{\rho_2^\theta-\rho_1^\theta}{2} = r, \forall\theta \in [0,\pi)$ is a circle of radius r.*

Proof Because of $\Lambda^\theta(\mathcal{D}) = \mathcal{R}_\mathcal{D}(\theta, \frac{\rho_1^\theta+\rho_2^\theta}{2})$, and thanks to the definition of $\Lambda^\theta(\mathcal{D})$, we have: $\underset{\rho}{\operatorname{argmax}}\big(\mathcal{R}_\mathcal{D}(\theta,\rho)\big) = \frac{\rho_1^\theta+\rho_2^\theta}{2}$. Because ρ_1^θ and ρ_2^θ are the borders of the "projected band" of $\mathcal{D}$ in direction θ, we have $\Delta_1^\theta(\mathcal{D}) = \frac{\rho_1+\rho_2}{2} - \rho_1 = \frac{\rho_2-\rho_1}{2}$ and $\Delta_2^\theta(\mathcal{D}) = \rho_2 - \frac{\rho_1+\rho_2}{2} = \frac{\rho_2-\rho_1}{2}$. Therefore, $\frac{1}{2}\Lambda^\theta(\mathcal{D}) = \Delta_1^\theta(\mathcal{D}) = \Delta_2^\theta(\mathcal{D}) = r, \forall\theta \in [0,\pi)$. By applying Proposition 2, we deduce that $\mathcal{D}$ is a circular disk of radius r.

Accordingly, based on Proposition 3, an improved definition of circularity measure is addressed in Definition 2 as follows.

Definition 2 Let us denote $U_\Theta^2(\mathcal{D}) = \{\frac{\Lambda^\theta(\mathcal{D})}{2}, \frac{1}{2}\mathcal{R}_\mathcal{D}(\theta, \frac{\rho_1^\theta+\rho_2^\theta}{2}), \frac{\rho_2^\theta(\mathcal{D})-\rho_1^\theta(\mathcal{D})}{2}\}_{\theta\in\Theta}$. The improved circularity measure of $\mathcal{D}$ is defined as

$$iCM(\mathcal{D}) = e^{-\frac{\sigma(U_\Theta^2(\mathcal{D}))}{\mu(U_\Theta^2(\mathcal{D}))}} \tag{5}$$

Algorithm 2 is then introduced to calculate circular measure by using Definition 2. It should be noted that a normalization step is addressed before the construction of profile $U_\Theta^2(\mathcal{D})$ by dividing all three above components by the last one $(\frac{\rho_2^\theta(\mathcal{D})-\rho_1^\theta(\mathcal{D})}{2})$ to make the measure more robust against change of scales. Although both these algorithms come theorically from Definition 1 , the second one overcomes the numerical issues raised in Algorithm 1. In practice, we observe that the obtained measure is more stable than that produced by the first algorithm by avoiding the estimation of $\Delta_1^\theta(\mathcal{D})$, $\Delta_2^\theta(\mathcal{D})$ which are numerical issues. Those do not influence on the alternative measurements: $\frac{\rho_2^\theta(\mathcal{D})-\rho_1^\theta(\mathcal{D})}{2}$, and $\frac{1}{2}\mathcal{R}_\mathcal{D}(\theta, \frac{\rho_1^\theta+\rho_2^\theta}{2})$.

Algorithm 2 Improved circularity measurement of a shape $\mathcal{D}$.

Input: $\mathcal{D}$ – arbitrary shape, n – number of projection directions
Output: $iCM(\mathcal{D})$ – improved circularity measure

1: $\Theta = \{\theta_i\}_{i=0}^{n-1}$, $\theta_i = i\frac{\pi}{n}$
2: Determine $\mathcal{R}(\mathcal{D})$ -Radon image of $\mathcal{D}$
3: **for** $\theta_i \in \Theta$ **do**
4: From $\mathcal{R}(\mathcal{D})$, determine $\Lambda^{\theta_i}(\mathcal{D})$, $\rho_2^{\theta_i}(\mathcal{D})$, $\rho_1^{\theta_i}(\mathcal{D})$, $\mathcal{R}_{\mathcal{D}}(\theta, \frac{\rho_1^{\theta_i}(\mathcal{D})+\rho_2^{\theta_i}(\mathcal{D})}{2})$
5: **end for**
6: $U_{\Theta}^2(\mathcal{D}) = \{u_i\}_{i=0}^{3n-1}$, where $u_j = \frac{\Lambda^{\theta_j}(\mathcal{D})}{\rho_2^{\theta_i}(\mathcal{D})-\rho_1^{\theta_i}(\mathcal{D})}$, $u_{j+2n} = \frac{\mathcal{R}_{\mathcal{D}}\left(\theta_i, \frac{\rho_1^{\theta_i}(\mathcal{D})+\rho_2^{\theta_i}(\mathcal{D})}{2}\right)}{\rho_2^{\theta_i}(\mathcal{D})-\rho_1^{\theta_i}(\mathcal{D})}$, $u_{j+2n} = 1, \forall 0 \leq j < n$
7: $\sigma(\mathcal{D}) = \frac{1}{3n}\sum_{i=0}^{3n-1} u_i$
8: $\mu(\mathcal{D}) = \sqrt{\frac{1}{3n}\sum_{i=0}^{3n-1}(u_i - \sigma(\mathcal{D}))^2}$
9: $iCM(\mathcal{D}) = e^{-\frac{\sigma(\mathcal{D})}{\mu(\mathcal{D})}}$

4.2 Complexity

Let us consider the input image of $M = m \times m$ pixels. The calculation of Algorithms 1, 2 could be separated into three steps: Radon transform, the estimation of profile $U_{\Theta}^1(\mathcal{D})$ (resp. $U_{\Theta}^2(\mathcal{D})$), the calculation of circularity measure from profile $U_{\Theta}^1(\mathcal{D})$ (resp. $U_{\Theta}^2(\mathcal{D})$). The Radon transform can be computed rapidly based on recursively defined digital straight lines [56] that requires only $M \times \log(M)$ operations. Please refer to [56] for more implementation details of fast Radon transform. The second step requires $O(nm) = O(n\sqrt{M})$ operations while the third step needs only $O(n)$ operations. On the other hand, because n is the number of considered projections, it can be seen as a constant (in practice, n is set to 180). Therefore, our methods (Algorithms 1 and 2) have a same complexity of $M \times \log(M)$.

4.3 Properties

4.3.1 Robustness to additive noise and distorted boundary

Based on the Radon transform, a degradation to shapes such as salt & pepper noise addition or boundary distortion only results in a small change in their C^{θ} profiles and therefore it leads to a small change in our measure, defined in Algorithm 2. As a consequence, the proposed measure is robust against such degradation. Figure 5 shows that $C^{\frac{\pi}{2}}$ only changes slightly when the circle boundary is distorted. Thus, the proposed circularity measure is robust against degradations of shape boundary.

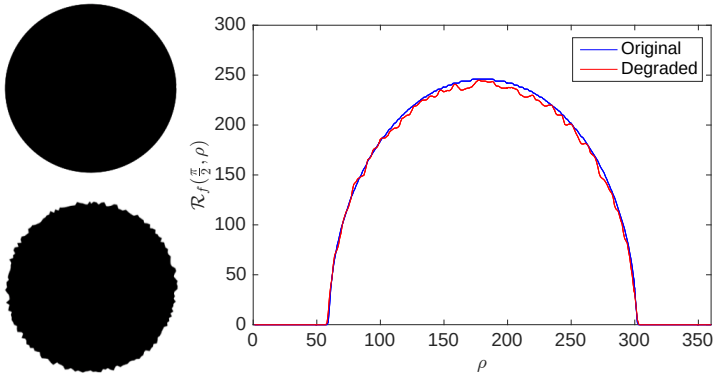

(a) Sample circles (b) Their $C^{\frac{\pi}{2}}$ profiles

Fig. 5: The $C^{\frac{\pi}{2}}$ profile of a circle and its boundary-distorted version.

4.3.2 Robustness to similarity transformation

From the last three properties of Radon transform in Section 3.1, the C^θ of a function f can be shown to have the following properties.

- A translation of f by a distance $\mathbf{x}_0$ does not change C_f^θ.
- A rotation of f by an angle θ_0 results in a shift in the index θ of C_f^θ by a distance θ_0: $C_f^\theta(\rho) \rightarrow C_f^{(\theta+\theta_0)}(\rho)$.
- A scaling of f by factor α results in the scaling in the variable ρ and the amplitude of C_f^θ: $C_f^\theta(\rho) \rightarrow \frac{1}{\alpha} C_f^\theta(\alpha\rho)$.

Our measure is introduced using extracted geometric features of C^θ. In order to make the proposed measure invariant to rotation, we consider C^θ at equidistant samples of $\theta \in [0, \pi)$. Our measure ensures the scaling invariance thanks to a simple normalization of deviation by r that is estimated as mean value of this sequence $\{u_i\}_{i=0}^{2n-1}$. Thus, the proposed circularity measure is invariant to translation, rotation, and scaling.

5 A novel evaluation criterion for assessing shape measures

To the best of our knowledge, although many circularity measures have been presented, there is not any evaluation criterion for comparing these measures like polygonalization [52,53]. There are many desired properties such as robustness to distortion, invariant against similarity transforms, etc to take into account a measure. Consider separately each property does not allow to obtain a general evaluation of such a measure.

We introduce then in this section such a criterion for this purpose by assessing the discriminant power of a shape measure. Our point of view is the following. *The better a shape measure is, the greater its discrimination power*

is. It means that using a good shape measure as a distance for shape classification on a dataset, we could observe the two following properties: i) the distances between inner classes must be small; ii) the distances between outer classes must be large.

Let us consider now a dataset S containing p groups of different shapes and each group has q sampled shapes. Suppose that S_{ij} $(1 \leq i \leq p, 1 \leq j \leq q)$ is the j^{th} sampled shape of the i^{th} group. Consider now a measure m, the obtained value using measure m on the shape S_{ij} is noted as $CM_m(S_{ij})$. The distribution of measured shapes within the i^{th} group is characterized by its mean and standard deviation values:

$$\mu_m^i(S) = \frac{1}{q}\sum_{j=1}^{q} CM_m(S_{ij}) \tag{6}$$

$$\sigma_m^i(S) = \sqrt{\frac{1}{q}\sum_{j=1}^{q}\Big(CM_m(S_{ij}) - \mu_m^i(S)\Big)^2} \tag{7}$$

By their definitions, $\mu_m^i(S)$ and $\sigma_m^i(S)$ can be seen respectively as the representative and dispersion values of the i^{th} group using measure m. In the following, we define the inner distance as the mean of dispersion values, the outer distance as the standard deviation of representative values of all groups of shapes.

$$InnerD_m(S) = \frac{1}{p}\sum_{i=1}^{p} \sigma_m^i(S) \tag{8}$$

$$OuterD_m(S) = \sqrt{\frac{1}{p}\sum_{j=1}^{p}\Big(\mu_m^i(S)) - \frac{1}{q}\sum_{j=1}^{q}\mu_m^i(S)\Big)^2} \tag{9}$$

We then propose an evaluation criterion as $POD_m(S)$ to measure the Power Of Discrimination on dataset S using shape measure m as follows.

$$POD_m(S) = \frac{OuterD_m(S)}{InnerD_m(S)} \tag{10}$$

This proposed criterion simply comes from our starting point of view: the better a measure m is; the larger the outer distance $OuterD_m(S)$ is and the smaller inner distance $InnerD_m(S)$ is.

6 Experiments

6.1 Circularity measurement on synthetic data

We have experimented our measure on synthetic data to consider its behavior in different conditions such as boundary distortion, noise, etc. Thanks to the projection-based approach, our method can deal with complex shapes

(a) (b) (c)

Fig. 6: Shapes composed of multiple closed contours taken from MPEG dataset.

(a) 0.805 (b) 0.514 (c) 0.467

Fig. 7: Experiments of iCM measure on compound shapes taken from [24].

composed of several closed contours like moment-based methods [24]. This is an important advantage compared with contour-based methods [57,27,28,29] requiring shapes represented by a unique closed contour that is not always satisfied in real conditions (see Figure 6). Figure 7 presents the obtained results on compound shapes. It also shows that for compound shapes the circularity value depends clearly on the mutual positions of their components even if the components are the same. In Figure 7, each shape contains 3 disconnected components where each component is a circle. It could be seen from this Figure that even each component is a circle in Figure 7, the measure is high when the components are concentrated on a center (Figure 7.a) while it is low when the components are on a line (Figures 7.b, 7.c) and in addition the lowest value is obtained when the components are far away from each other (Figure 7.c). It seems that this result corresponds well to the intuition of human visual perception.

We also consider the proposed measure on the shapes suffering different levels of boundary distortion. Figures 8 and 9 present the experiments on both non-circular and circular shapes. It could be seen that the proposed measure is robust against various levels of boundary distortion.

From these experiments, we could make the following findings.

- The circularity measures of similar shapes come closer to a value.
- Two shapes having a same circularity measure are not necessarily similar.

(a) 0.766 (b) 0.774 (c) 0.771 (d) 0.777

Fig. 8: Experiments on non-circular shape under different levels of boundary distortion using our iCM measure. The shapes are taken from [24]

(a) 0.986 (b) 0.989 (c) 0.965

Fig. 9: Experiments on circular shape under different level of boundary distortion using our iCM measure.

6.2 Circularity measurement on real data

The proposed circularity measure has also been evaluated on different following shape datasets which consist of object shapes segmented from real images.

- Kimia 99 dataset [58]: This consists of 99 shapes, decomposed into 9 classes, and each class contains 11 different shapes (see Figure 10).
- Sharvit dataset [59]: This contains 256 shapes, grouped in 18 categories, and each category consists of 12 shapes (see Figure 13 for several shape examples).
- Floral dataset: We have also designed Floral dataset [1] in order to evaluate how the proposed method deal with compound shapes and how robust it is against noise influence. It consists of 20 basic floral shapes which are all compound shapes. Based on each basic shape, a series of 10 noise shapes is generated by addressing different levels of noise (i. e. SNR=$\{1, 1.5, 2, 2.5, 3, 3.5, 4, 4.5, 5, 5.5\}$). Finally, the dataset contains 20 classes, each class is structured from a basic floral shape and its 10 corresponding noise versions. Figure 11 presents 20 basic floral shapes while Figure 12 illustrates 20 derived shapes at noise level SNR=1.

Figure 10 reports the results on Kimia dataset using our circularity measure (iCM) while Figure 13 presents the our results on several shapes of Sharvit

[1] This can be publicly accessed at address `http://tpnguyen.univ-tln.fr/download/floral_dataset`

Table 1: Influence of the angular sampling step on our measure iCM.

Shape	$\triangle\theta$ (degree)							Mean	Std
	1	2	4	6	8	16	32		
Fig. 7.a	0.805	0.804	0.804	0.802	0.804	0.803	0.803	0.804	0.0011
Fig. 7.b	0.514	0.514	0.514	0.515	0.509	0.528	0.516	0.516	0.0056
Fig. 7.c	0.467	0.467	0.466	0.466	0.462	0.479	0.466	0.468	0.0051
Fig. 8.a	0.766	0.765	0.763	0.763	0.765	0.762	0.766	0.764	0.0015
Fig. 8.b	0.774	0.774	0.772	0.770	0.771	0.771	0.776	0.773	0.0023
Fig. 8.c	0.771	0.770	0.769	0.768	0.769	0.768	0.771	0.769	0.0015
Fig. 8.d	0.777	0.776	0.774	0.775	0.774	0.773	0.771	0.774	0.0020

Table 2: Comparison on robustness to distortion boundary.

Shape	Rosenfeld	Haralick	Bribiesca	Danielsson	Ruberto and Dempster	Zunic *et al.*	Ours (iCM)
Fig. 8.a	0.3232	0.6687	0.9941	0.3077	0.2977	0.7473	0.766
Fig. 8.b	0.2438	0.6665	0.9887	0.2717	0.6052	0.7559	0.774
Fig. 8.c	0.1694	0.6716	0.9887	0.2494	0.4307	0.7583	0.771
Fig. 8.d	0.1097	0.6889	0.9835	0.1950	0.6239	0.7456	0.777

dataset. It could be seen from this experiment that the intra-distance between shapes of the same class is sufficiently smaller than the inter-distance between shapes from different classes. Thus, the proposed circularity measure can be used as features in shape recognition problems. On the other hand, Tables 4, 5,6 present the discriminant power of our proposed measures (CM and iCM) on datasets Sharvit, Kimia 99, and Floral respectively. From these tables, it could be noted that although two measures are defined from equivalent definitions but the improved measure (iCM) is more robust against deformations because it has not numerical issues in calculation as the previous one (CM).

6.3 Influence of the angular sampling step

We have investigated the influence of θ sampling step in Radon transform to the proposed measures. For this purpose, we calculated the circularity measure for different shapes in Figures 7 and 8 at a number of sampling steps: $\triangle\theta = 1, 2, 4, 6, 8, 16, 32$ (degree). Table 1 shows the obtained values. It could be seen from Table 1 the following important remarks.

1. The proposed measure doesn't change very much while $\triangle\theta$ increases from 1 to 16; and that considerable changes can only be observed when $\triangle\theta$ increases from 16 to 32. This allow us to optimize the number of projected directions. If $\triangle\theta$ is set to 16, we only need 11 projections to calculate the circularity measure instead of using 180 projections as usual.
2. The influence of the angular sampling step is less than that of boundary distortion.

6.4 Comparison with existing measures

We compare our measure with other existing circularity measures : Rosenfeld [60], Haralick [19], Bribiesca [30], Danielsson [20], Ruberto and Dempster[21],

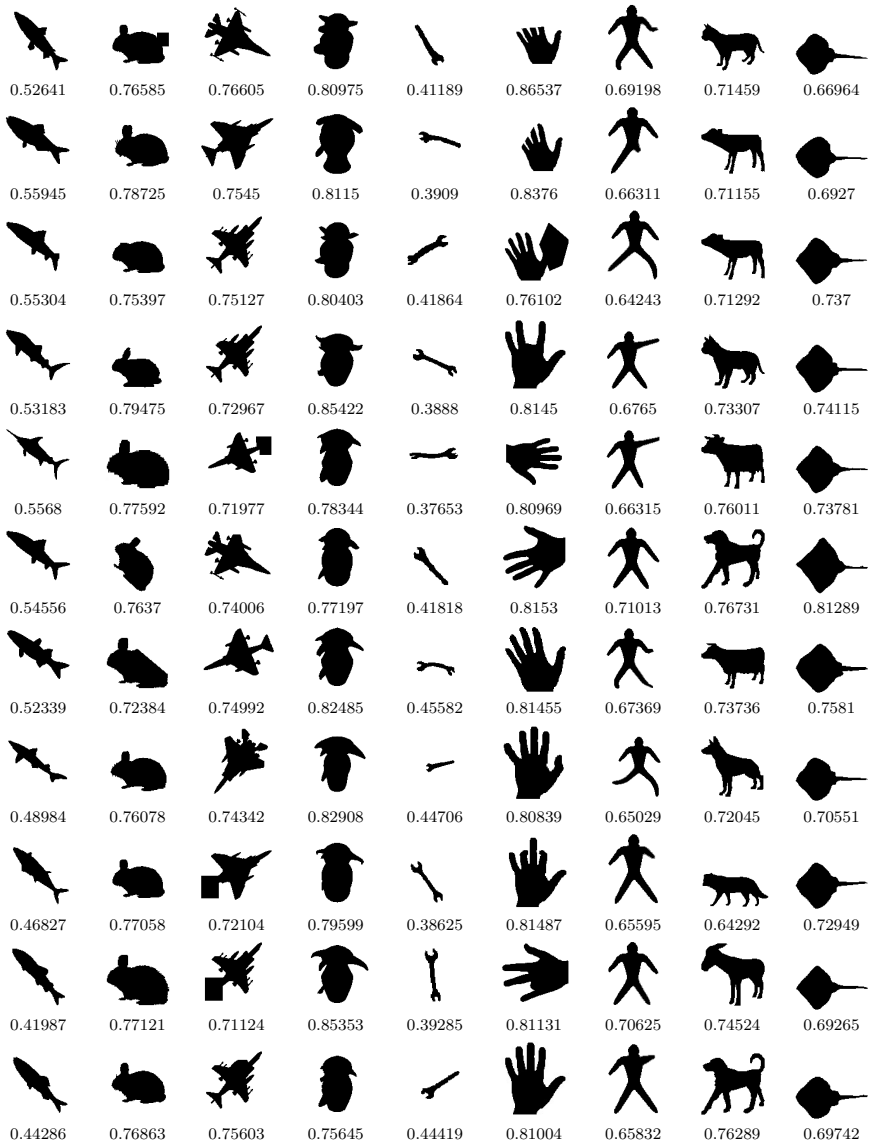

Fig. 10: Kimia 99 dataset.

Zunic *et al.* [24]. We have evaluated our measure in comparison with those measures on the following different datasets: Kimia [58], Sharvit [59], and our Floral. The two first datasets are well-known considered for evaluation of shape descriptors. The last one is introduced to address compound shapes and noise conditions. Table 3 presents the distribution (mean and std) of different methods on each group of Kimia dataset. We can make several findings from

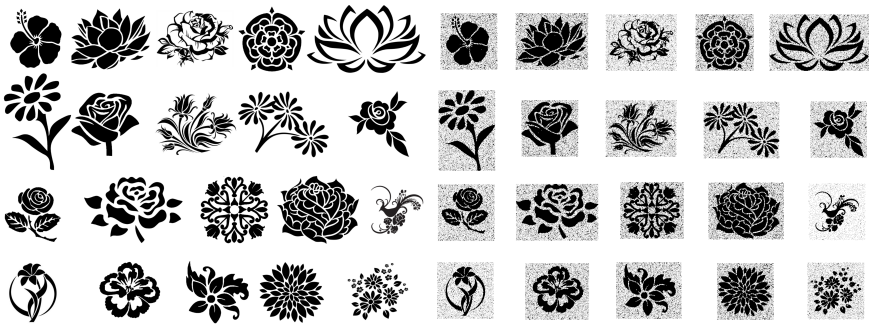

Fig. 11: Floral dataset: Basic shapes.

Fig. 12: Floral dataset: Noisy shapes.

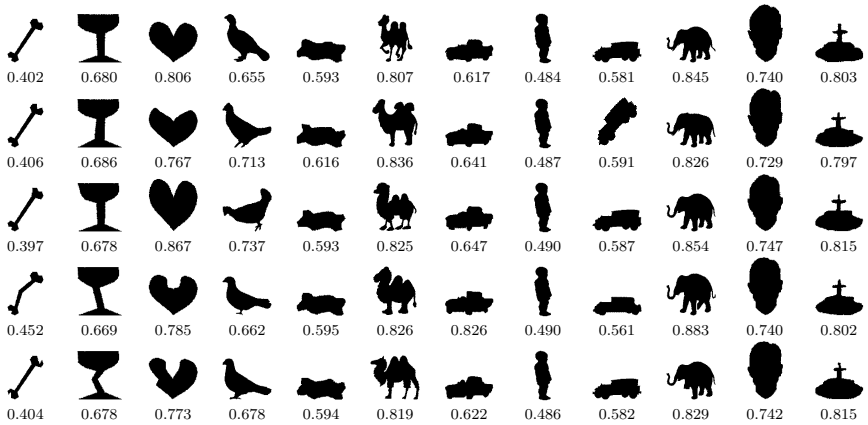

Fig. 13: Some shapes of Sharvit dataset.

this table. First, our measure can distinguish shapes from different groups since each group can be characterized by its mean value of circularity. Second, our measure tolerates well the shapes belonging to a same groups since the inner-class distances, defined by variance value of circularity, are relatively small. In addition, Tables 4, 5,6 show the POD criterion of each measure on three above datasets to address its discrimination power. It could be seen from them that our improved measure (iCM) together with Zunic *et al.*'s measure are more efficient than others. Moreover, thanks to a similar computational framework, we can easily integrate the proposed measure and our previous work on polygonality [31] for shape classification without increasing practically the computation cost.

6.5 Application to linearity measuring

Inspired from [24], we also consider a direct application of circularity measurement in linearity measuring. A shape, measured with a very low circularity

Table 3: Measured values of different methods on each group of shape of Kimia 99 dataset.

Groupe of shapes	Rosenfeld	Haralick	Bribiesca	Danielsson	Ruberto and Dempester	Zunic et al.	Ours (iCM)
Fish	0.171 ± 0.029	0.545 ± 0.023	0.974 ± 0.007	0.197 ± 0.023	0.486 ± 0.317	0.397 ± 0.053	0.511 ± 0.048
Rabbit	0.359 ± 0.044	0.784 ± 0.018	0.992 ± 0.001	0.427 ± 0.038	0.704 ± 0.180	0.825 ± 0.028	0.767 ± 0.018
Plane	0.117 ± 0.026	0.659 ± 0.032	0.973 ± 0.006	0.192 ± 0.026	0.551 ± 0.185	0.639 ± 0.042	0.740 ± 0.018
Fgen	0.315 ± 0.043	0.779 ± 0.018	0.992 ± 0.002	0.389 ± 0.045	0.515 ± 0.172	0.821 ± 0.027	0.809 ± 0.031
Hand	0.155 ± 0.025	0.509 ± 0.024	0.947 ± 0.006	0.187 ± 0.031	0.520 ± 0.244	0.228 ± 0.036	0.412 ± 0.027
Tool	0.156 ± 0.022	0.731 ± 0.031	0.983 ± 0.002	0.232 ± 0.031	0.390 ± 0.228	0.767 ± 0.029	0.815 ± 0.025
Dude	0.106 ± 0.009	0.625 ± 0.019	0.967 ± 0.001	0.136 ± 0.012	0.845 ± 0.005	0.465 ± 0.025	0.672 ± 0.022
Animal	0.131 ± 0.025	0.686 ± 0.026	0.975 ± 0.004	0.214 ± 0.058	0.444 ± 0.257	0.575 ± 0.052	0.728 ± 0.035
Batoidea	0.292 ± 0.013	0.657 ± 0.041	0.989 ± 0.001	0.414 ± 0.016	0.651 ± 0.221	0.804 ± 0.036	0.725 ± 0.040

Table 4: POD criterion of different methods on the Sharvit dataset.

Rosenfeld	Haralick	Bribiesca	Danielsson	Ruberto and Dempster	Zunic *et al.*	Ours (iCM)
4.08	4.19	4.73	3.47	0.28	5.74	5.74

Table 5: Experiment on Kamia 99 dataset using POD criterion.

Bribiesca	Danielson	Haralick	Zunic *et al.*	Rosenfeld	Ours (CM)	Ours (iCM)
4.21	3.63	3.69	5.88	3.63	4.04	4.67

Table 6: Evaluation on Floral dataset using POD criterion.

Bribiesca	Danielson	Haralick	Zunic *et al.*	Rosenfeld	Ours (CM)	Ours (iCM)
0.002239	0.041807	0.031641	0.045099	0.018785	0.0303	0.0692

value, is intuitively expected to be more linear. Figure 14 presents several linear shapes together with their circularity measure. It could be seen that the more a shape is linear the more its circularity measure is small. Therefore, $1-CM(\mathcal{D})$ is a suggestion to measure the linearity of a shape. Figure 15 shows the profile of circularity measures obtained from a set of ellipses of which the minor axis is varied from 1 to 200, the major axis is set to 200. We also consider the profile of circularity measures in Figure 16 obtained from a set of rectangles of which the width is set to 300, the height varies from 1 to 300. Figure 16.b presents one rectangle of this set; its height is 30 and its measure is 0.207. From those profiles, we could make the following observations. The ellipses of which the minor axis is less than or equal to 20 have small circularity measure (less than 0.2). Similarly, the rectangle of which the height is less than or equal to 30 have circularity measure less than 0.2 too. In other word, using our proposed circularity measure, a shape can be seen as a linear shape having a ratio width/length less than 10% if its circularity measure is relatively small. Thus, a threshold from 0.2 to 0.25 can be considered to detect linear shapes by addressing our iCM circularity measure.

7 Conclusions

We have presented a new circularity measure that is invariant against similarity transforms such as translation, rotation and scaling. In addition, it is robust

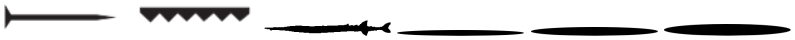

(a) 0.288 (b) 0.251 (c) 0.205 (d) 0.071 (e) 0.111 (f) 0.175

Fig. 14: Circularity measurement on linear shapes using iCM measure. The shapes a), b) are taken from [24].

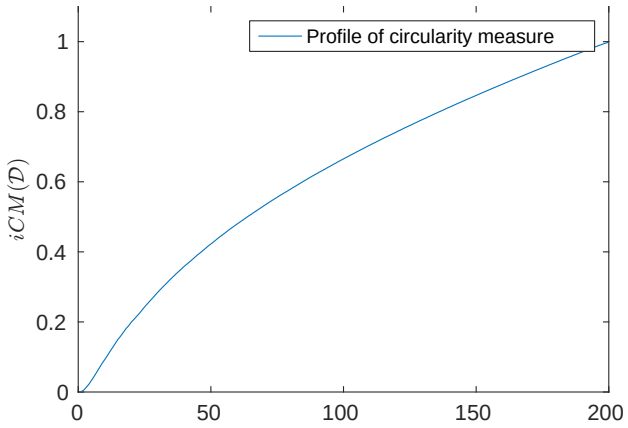

Fig. 15: Profile of circularity measures obtained from a set of ellipses of which the major axis is set to 200, the minor axis is varied from 1 to 200.

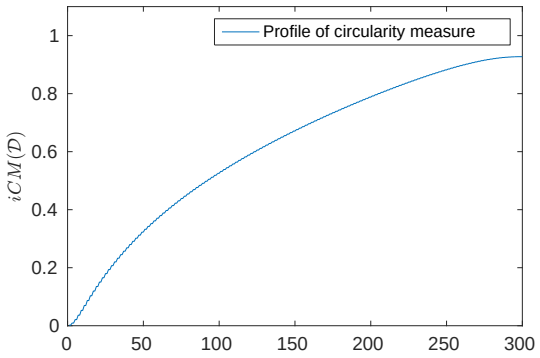

(a)

(b) $iCM = 0.207$

Fig. 16: (a): Profile of circularity measures obtained from a set of rectangle of which the width is set to 300, the height is varied from 1 to 300; (b): A rectangle of height 30, width 300

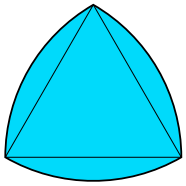

Fig. 17: Reuleaux triangle.

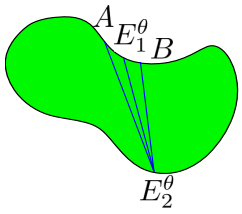

Fig. 18: Lemma 1.

with respect to distortion on boundary shape. The proposed measure is shown to be a good feature for shape description. We have also introduced a new evaluation criterion for evaluating and comparing different shape measures by assessing their power of discrimination. In the future, we are interested in extending this approach for other problems in shape measurement such as rectangularity, ellipticity, etc.

Acknowledgements

We are grateful to two reviewers for kindly providing us their valuable and insightful comments to improve the manuscript.

A Materials for the inverse problem

The following lemmas establishes the relation between convex and non-convex shapes as well as the properties of a convex shape satisfying the conditions in Proposition 2.

Lemma 1 *If an arbitrary shape $\mathcal{D}$ satisfies this condition: $\frac{1}{2}\Lambda^\theta(\mathcal{D}) = \Delta_1^\theta(\mathcal{D}) = \Delta_2^\theta(\mathcal{D}) = r, \forall\theta \in [0,\pi)$, its convex hull $CV(\mathcal{D})$ satisfies the above condition too.*

Proof First, we will prove that any extremity E_1^θ, E_2^θ is not in a concave part of the boundary of $\mathcal{D}$ for any direction θ. Suppose that E_1^θ is in concave part. It means that there exists 2 points A, B on the boundary of $\mathcal{D}$ nearby E_1^θ at the left and right sides such that E_1^θ is inside of triangle $E_2^\theta AB$ (see Figure 18). So, $\max(AE_2^\theta, BE_2^\theta) > E_1^\theta E_2^\theta = 2r$. This fact is contradictory to the above condition of $\mathcal{D}$. On the other hand, it is evident that $\mathcal{D}$ and its convex hull $CV(\mathcal{D})$ have a same projected band in any direction. From the two above facts, we can deduce the conclusion of this lemma.

Lemma 2 *Let us denote the two extremities in the boundary of $\mathcal{D}$ corresponding to $\rho_0^\theta(\mathcal{D})$ as E_1^θ and E_2^θ, respectively (see also Section 3.1.2 for more detail). $E_1^\theta E_2^\theta$ and $E_1^{\theta+\frac{\pi}{2}} E_2^{\theta+\frac{\pi}{2}}$ intersect at the midpoint of each segment $\forall\theta \in [0, \frac{\pi}{2})$.*

Proof Let us consider direction θ, we have the following condition: $E_1^\theta E_2^\theta = 2r$ because of $\frac{1}{2}\Lambda^\theta(\mathcal{D}) = r$. Therefore, in direction $\theta + \frac{\pi}{2}$, the length of $\mathcal{D}$ is at least $2r$, the minimal value is obtained when E_1^θ and E_2^θ must be on the two supporting lines of $\mathcal{D}$ in this direction, respectively. In Figure 19, these supporting lines, namely d_1 and d_2, are perpendicular with $E_1^\theta E_2^\theta$ at E_1^θ and E_2^θ respectively. In addition, $\Delta_1^{\theta+\frac{\pi}{2}}(\mathcal{D}) + \Delta_2^{\theta+\frac{\pi}{2}}(\mathcal{D}) = 2r$. Therefore, in direction $\theta + \frac{\pi}{2}$, the projected band of $\mathcal{D}$ must be sandwiched between two lines d_1 and d_2 (see Figure 19).

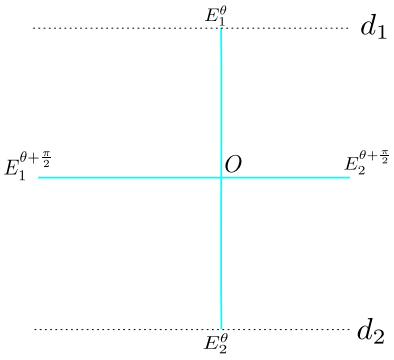

Fig. 19: Lemma 2.

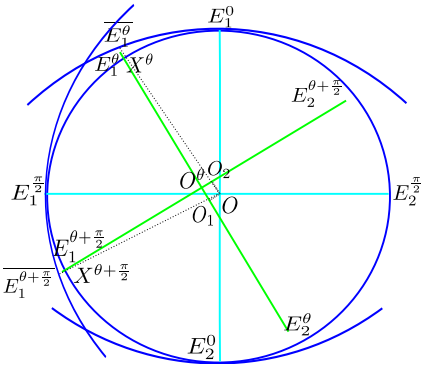

Fig. 20: Lemma 3.

Because of $\Delta_1^\theta(\mathcal{D}) = \Delta_2^\theta(\mathcal{D}) = r, \forall\theta \in [0,\pi)$, $E_1^{\theta+\frac{\pi}{2}}E_2^{\theta+\frac{\pi}{2}}$ must be equidistant from d_1 and d_2. So, we have $E_1^\theta O = E_2^\theta O$. Similarly, by considering direction $\theta+\frac{\pi}{2}$, we obtain $E_1^{\theta+\frac{\pi}{2}}O = E_2^{\theta+\frac{\pi}{2}}O$.

Lemma 3 *Suppose that O (resp. O^θ) is the intersection between $E_1^0E_2^0$ and $E_1^{\frac{\pi}{2}}E_2^{\frac{\pi}{2}}$ (resp. $E_1^\theta E_2^\theta$ and $E_1^{\theta+\frac{\pi}{2}}E_2^{\theta+\frac{\pi}{2}}$) (please see Section 3.1.2 for the definitions of E_1^θ and E_2^θ). We have following property: $OO^\theta \leq \sqrt{2}r(\sqrt{5-4\cos(\theta)}-1)$*

Proof Lemma 2 allows to deduce that the border of $\mathcal{D}$ is decomposed into a set of tuples $(E_1^\theta, E_2^\theta, E_1^{\theta+\frac{\pi}{2}}, E_2^{\theta+\frac{\pi}{2}})$ where the intersection O^θ is the midpoints of two segments $E_1^\theta E_2^\theta$, $E_1^{\theta+\frac{\pi}{2}}E_2^{\theta+\frac{\pi}{2}}$. Suppose that $\zeta(O,r)$ is the circle of center O, of radius r. Without loss of generality, suppose that O^θ is in the fourth octant (see Figure 20). In addition, for the simplicity of presentation, we consider $\theta \leq \frac{\pi}{4}$, the other cases can be considered similarly. We then denote O_1 (resp. O_2) the projection of O on $E_1^\theta E_2^\theta$ (resp. $E_1^{\theta+\frac{\pi}{2}}E_2^{\theta+\frac{\pi}{2}}$); X^θ and $\overline{E_1^\theta}$ (resp. $X^{\theta+\frac{\pi}{2}}$ and $\overline{E_1^{\theta+\frac{\pi}{2}}}$) are the intersections between OE_1^θ (resp. $OE_1^{\theta+\frac{\pi}{2}}$) and $\zeta(O,r)$ and $\zeta(E_2^0,2r)$ (resp. $\zeta(O,r)$ and $\zeta(E_2^{\frac{\pi}{2}},2r)$).

In this condition, it is evident to deduce that E_1^θ and $E_1^{\theta+\frac{\pi}{2}}$ are outside or on the boundary of $\zeta(O,r)$. In addition, because of the length of $\mathcal{D}$ in any direction is a constant $(2r)$, we deduce that $E_2^0E_1^\theta \leq 2r$ and $E_2^{\frac{\pi}{2}}E_1^{\theta+\frac{\pi}{2}} \leq 2r$. Therefore, E_1^θ (resp. $E_1^{\theta+\frac{\pi}{2}}$) must be in the small zone determined by 3 circles: $\zeta(O,r)$, $\zeta(E_2^0,2r)$, $\zeta(E_2^{\frac{\pi}{2}},2r)$ (resp. $\zeta(O,r)$, $\zeta(E_1^0,2r)$, $\zeta(E_2^{\frac{\pi}{2}},2r)$) (see also Figure 20). So, we have:

$$E_1^\theta X^\theta \leq \overline{E_1^\theta}X^\theta \text{ and } E_1^{\theta+\frac{\pi}{2}}X^{\theta+\frac{\pi}{2}} \leq \overline{E_1^{\theta+\frac{\pi}{2}}}X^{\theta+\frac{\pi}{2}} \tag{11}$$

Moreover, because O_1 and O_2 are projections of O, it is evident that $E_1^\theta O_1 \leq E_1^\theta O \Leftrightarrow E_1^\theta O^\theta + O^\theta O_1 \leq E_1^\theta X^\theta + X^\theta O \Leftrightarrow r + O^\theta O_1 \leq E_1^\theta X^\theta + r \Leftrightarrow O^\theta O_1 \leq E_1^\theta X^\theta$ and $E_1^{\theta+\frac{\pi}{2}}O_2 \leq E_1^{\theta+\frac{\pi}{2}}O \Leftrightarrow E_1^{\theta+\frac{\pi}{2}}O^\theta + O^\theta O_2 \leq E_1^{\theta+\frac{\pi}{2}}X^{\theta+\frac{\pi}{2}} + X^{\theta+\frac{\pi}{2}}O \Leftrightarrow r + O^\theta O_2 \leq E_1^{\theta+\frac{\pi}{2}}X^{\theta+\frac{\pi}{2}} + r \Leftrightarrow O^\theta O_2 \leq E_1^{\theta+\frac{\pi}{2}}X^{\theta+\frac{\pi}{2}}$. Briefly, we have:

$$O^\theta O_1 \leq E_1^\theta X^\theta \text{ and } O^\theta O_2 \leq E_1^{\theta+\frac{\pi}{2}}X^{\theta+\frac{\pi}{2}} \tag{12}$$

Consider now the triangle $\overline{E_1^\theta}OE_2^0$, we have

$\overline{E_1^\theta}O = \sqrt{|\overline{E_1^\theta}E_2^0|^2 + |OE_2^0|^2 - 2|\overline{E_1^\theta}E_2^0||OE_2^0|\cos(\angle\overline{E_1^\theta}E_2^0O)} \Leftrightarrow \overline{E_1^\theta}X^\theta + r = \sqrt{5r^2 - 4r^2\cos(\angle\overline{E_1^\theta}E_2^0O)}$

$\Leftrightarrow \overline{E_1^\theta X^\theta} = r(\sqrt{5-4\cos(\angle\overline{E_1^\theta E_2^0 O})}-1)$. Because of $\angle\overline{E_1^\theta E_2^0 O} \leq \theta$, we deduce that $\overline{E_1^\theta X^\theta} \leq r(\sqrt{5-4\cos(\theta)}-1)$. Similarly, by considering the triangle $\overline{E_1^{\theta+\frac{\pi}{2}} O E_2^{\frac{\pi}{2}}}$, the following remarks is obtained.

$$\overline{E_1^\theta X^\theta} \text{ and } \overline{E_1^{\theta+\frac{\pi}{2}}} X^{\theta+\frac{\pi}{2}} \leq r(\sqrt{5-4\cos(\theta)}-1) \tag{13}$$

Using the results in Inequations (11), (12), (13), we have the conclusion of this lemma: $OO^\theta = \sqrt{|OO_1|^2+|OO_2|^2} \leq \sqrt{2}r(\sqrt{5-4\cos(\theta)}-1)$.

Lemma 4 $\lim\limits_{n\to+\infty} n(\sqrt{5-4\cos(\frac{\pi}{4n})}-1) = 0$

Proof Due to Taylor's series, we have $1-\frac{x^2}{2} \leq cos(x) \leq 1$, therefore $1 \leq 5-4\cos(x) \leq 1+2x^2 \leq (1+x^2)^2$. So, we have $0 \leq \sqrt{5-4\cos(x)}-1 \leq x^2$. Replacing x by $\frac{\pi}{4n}$, we obtain the following result $0 \leq n(\sqrt{5-4\cos(\frac{\pi}{4n})}-1) \leq \frac{\pi^2}{16n}$. It is evident that $\lim\limits_{n\to+\infty} \frac{\pi^2}{16n} = 0$. This fact proves our conclusion.

References

1. P. L. Rosin, Measuring shape: ellipticity, rectangularity, and triangularity, Mach. Vis. Appl. 14 (3) (2003) 172–184.
2. E. T. Bowman, K. Soga, T. Drummond, Particle shape characterization using Fourier analysis, Geotechnique 51 (6) (2001) 545–554.
3. D. H. Ballard, Generalizing the Hough transform to detect arbitrary shapes, Pattern Recognition 13 (2) (1981) 111–122.
4. T. V. Hoang, S. Tabbone, The generalization of the R-transform for invariant pattern representation, Pattern Recognition 45 (6) (2012) 2145–2163.
5. T. P. Nguyen, I. Debled-Rennesson, A discrete geometry approach for dominant point detection, Pattern Recognition 44 (1) (2011) 32–44.
6. E. Roman-Rangel, C. Wang, S. Marchand-Maillet, Simmap: Similarity maps for scale invariant local shape descriptors, Neurocomputing 175 (2016) 888 – 898.
7. A. B. Hamza, A graph-theoretic approach to 3d shape classification, Neurocomputing 211 (2016) 11 – 21.
8. T. V. Hoang, S. Tabbone, Errata and comments on "Generic orthogonal moments: Jacobi–Fourier moments for invariant image description", Pattern Recognition 46 (11) (2013) 3148–3155.
9. L. Kurnianggoro, Wahyono, K.-H. Jo, A survey of 2d shape representation: Methods, evaluations, and future research directions, Neurocomputing 300 (2018) 1 – 16.
10. D. Zhang, G. Lu, A comparative study of curvature scale space and Fourier descriptors for shape-based image retrieval, Journal of Visual Communication and Image Representation 14 (2003) 39–57.
11. M. Carlin, Measuring the performance of shape similarity retrieval methods, Comput. Vis. Image Underst. 84 (1) (2001) 44–61.
12. K. Nasreddine, A. Benzinou, R. Fablet, Variational shape matching for shape classification and retrieval, Pattern Recognition Letters 31 (12) (2010) 1650–1657.
13. L. Chen, R. S. Feris, M. Turk, Efficient partial shape matching using smith-waterman algorithm, in: IEEE Conference on Computer Vision and Pattern Recognition, CVPR Workshops 2008, Anchorage, AK, USA, 23-28 June, 2008, 2008, pp. 1–6.
14. M. Cui, J. Femiani, J. Hu, P. Wonka, A. Razdan, Curve matching for open 2d curves, Pattern Recognition Letters 30 (1) (2009) 1–10.
15. A. Leborgne, J. Mille, L. Tougne, Hierarchical skeleton for shape matching, in: ICIP, 2016, pp. 3603–3607.
16. D. Proffitt, The measurement of circularity and ellipticity on a digital grid, Pattern Recognition 15 (5) (1982) 383–387.

17. M. Peura, J. Iivarinent, Efficiency of simple shape descriptors, in: Aspects of visual form processing, 1997, pp. 443–451.
18. A. Rosenfeld, Compact figures in digital pictures, IEEE Trans. on Systems, Man and Cybernetics 4 (1974) 221–223.
19. R. Haralick, A measure for circularity of digital figures, IEEE Trans. Systems, Man, and Cybernetics 4 (1974) 394–396.
20. P. E. Danielsson, A new shape factor, Computer Graphic and Image Processing 7 (2) (1978) 292–299.
21. C. Di Ruberto, A. Dempster, Circularity measures based on mathematical morphology, Electronics Letters 36 (20) (2000) 1691–1693.
22. D. Proffitt, The measurement of circularity and ellipticity on a digital grid, Pattern Recognition 15 (1982) 383–387.
23. P. Rosin, Measuring shape: ellipticity, rectangularity, and triangularity, Machine Vision and Applications 14 (2003) 172–184.
24. J. D. Zunic, K. Hirota, P. L. Rosin, A Hu Moment Invariant as a Shape Circularity Measure, Pattern Recognition 43 (1) (2010) 47–57.
25. A. Stojmenovic, M.; Nayak, Shape based circularity measures of planar point sets, in: ICSPC, 2007, pp. 1279–1282.
26. N. Ritter, J. R. Cooper, New resolution independent measures of circularity, Journal of Mathematical Imaging and Vision 35 (2) (2009) 117–127.
27. S. Fisk, Separating point sets by circles, and the recognition of digital disks, IEEE Trans. Pattern Anal. Mach. Intell. 8 (4) (1986) 554 –556.
28. T. Roussillon, I. Sivignon, L. Tougne, Measure of circularity for parts of digital boundaries and its fast computation, Pattern Recognition 43 (1) (2010) 37–46.
29. T. P. Nguyen, I. Debled-Rennesson, Circularity measuring in linear time, in: ICPR, 2010, pp. 2098–2101.
30. E. Bribiesca, An easy measure of compactness for 2d and 3d shapes, Pattern Recognition 41 (2) (2008) 543–554.
31. T. P. Nguyen, T. V. Hoang, Projection-based polygonality measurement, IEEE Transactions on Image Processing 24 (1) (2015) 305–315.
32. D. Zunic, C. Martinez-Ortiz, J. D. Zunic, Shape rectangularity measures, IJPRAI 26 (6) (2012) 1–23.
33. C. Martinez-Ortiz, J. D. Zunic, Curvature weighted gradient based shape orientation, Pattern Recognition 43 (9) (2010) 3035–3041.
34. J. D. Zunic, Milosmenovic, Boundary based shape orientation, Pattern Recognition 41 (5) (2008) 1768–1781.
35. J. L. C. Sanz, I. Dinstein, Projection-based geometrical feature extraction for computer vision: algorithms in pipeline, IEEE Trans. Pattern Anal. Mach. Intell. 9 (1) (1987) 160–168.
36. V. F. Leavers, Use of the Radon transform as a method of extracting information about shape in two dimensions, Image and Vision Computing 10 (2) (1992) 99–107.
37. K. Jafari-Khouzani, H. Soltanian-Zadeh, Radon transform orientation estimation for rotation invariant texture analysis, IEEE Trans. Pattern Anal. Mach. Intell. 27 (6) (2005) 1004–1008.
38. E. Baudrier, M. Tajine, A. Daurat, Polygonal estimation of planar convex-set perimeter from its two projections, Discrete Applied Mathematics 161 (15) (2013) 2252–2268.
39. H. Hjouj, D. W. Kammler, Identification of reflected, scaled, translated, and rotated objects from their Radon projections, IEEE Transactions on Image Processing 17 (3) (2008) 301–310.
40. J. D. Zunic, P. L. Rosin, An alternative approach to computing shape orientation with an application to compound shapes, International Journal of Computer Vision 81 (2) (2009) 138–154.
41. R. K. K. Yip, Genetic Fourier descriptor for the detection of rotational symmetry, Image Vision Comput. 25 (2) (2007) 148–154.
42. Z. Xiao, Z. Hou, C. Miao, J. Wang, Using phase information for symmetry detection, Pattern Recognition Letters 26 (13) (2005) 1985–1994.
43. G. Tzimiropoulos, N. Mitianoudis, T. Stathaki, A unifying approach to moment-based shape orientation and symmetry classification, IEEE Transactions on Image Processing 18 (1) (2009) 125–139.

44. P. L. Rosin, J. Pantovic, J. D. Zunic, Measuring linearity of connected configurations of a finite number of 2d and 3d curves, Journal of Mathematical Imaging and Vision 53 (1) (2015) 1–11.
45. P. L. Rosin, J. Pantovic, J. D. Zunic, Measuring linearity of curves in 2d and 3d, Pattern Recognition 49 (2016) 65–78.
46. S. Pal, P. Bhowmick, Determining digital circularity using integer intervals, Journal of Mathematical Imaging and Vision 42 (1) (2012) 1–24.
47. Z. Ma, J. Ma, B. Xiao, K. Lu, A 3d polar-radius-moment invariant as a shape circularity measure, Neurocomputing 259 (2017) 140 – 145.
48. K. Misztal, J. Tabor, Ellipticity and circularity measuring via kullback-leibler divergence, Journal of Mathematical Imaging and Vision 55 (1) (2016) 136–150.
49. C. E. Kim, T. A. Anderson, Digital disks and a digital compactness measure, in: STOC, 1984, pp. 117–124.
50. P. L. Rosin, Measuring rectangularity, Mach. Vis. Appl. 11 (4) (1999) 191–196.
51. P. L. Rosin, J. D. Zunic, Measuring squareness and orientation of shapes, Journal of Mathematical Imaging and Vision 39 (1) (2011) 13–27.
52. D. Sarkar, A simple algorithm for detection of significant vertices for polygonal approximation of chain-coded curves, Pattern Recogn. Lett. 14 (12) (1993) 959–964.
53. P. L. Rosin, Techniques for assessing polygonal approximations of curves, IEEE Trans. Pattern Anal. Mach. Intell. 19 (6) (1997) 659–666.
54. S. Tabbone, O. R. Terrades, S. Barrat, Histogram of radon transform. A useful descriptor for shape retrieval, in: ICPR, 2008, pp. 1–4.
55. S. R. Deans, The Radon Transform and Some of Its Applications, Krieger Publishing Company, 1983.
56. M. L. Brady, A fast discrete approximation algorithm for the radon transform, SIAM J. Comput. 27 (1) (1998) 107–119.
57. C. E. Kim, T. A. Anderson, Digital disks and a digital compactness measure, in: Proc. STOC, 1984, pp. 117–124.
58. T. B. Sebastian, P. N. Klein, B. B. Kimia, Recognition of shapes by editing their shock graphs, IEEE Trans. Pattern Anal. Mach. Intell. 26 (5) (2004) 550–571.
59. D. Sharvit, J. Chan, H. Tek, B. B. Kimia, Symmetry-based indexing of image databases, Journal of Visual Communication and Image Representation 9 (1998) 366–380.
60. A. Rosenfeld, Compact figures in digital pictures, IEEE Transactions on Systems, Man and Cybernetics SMC4 (1974) 221–223.